LA-UR-15-28482
Approved for public release; distribution is unlimited.

Title: Colloid-Facilitated Transport of 137Cs in Fracture-Fill Material: Experiments and Modeling

Author(s): Dittrich, Timothy M.
Reimus, Paul William

Intended for: Report

Issued: 2015-10-29

7 Colloid-Facilitated Transport of ^{137}Cs in Fracture-Fill Material: Experiments and Modeling

7.1 Introduction

The most likely mechanism for strongly-adsorbing radionuclides to be transported significant distances in groundwater after being released from waste packages in a high-level nuclear waste repository is by colloid-facilitated transport. Baring a strong association with mobile colloids, strongly-adsorbing radionuclides are generally predicted to have negligible impact on dose estimates in repository risk assessments because they aren't expected to transport far enough to reach potential receptors. The objective of this study was to quantify the potential for colloid-facilitated transport of one strongly-adsorbing radionuclide, cesium (as ^{137}Cs), through a weathered fractured granodiorite system. Cs was adsorbed to bentonite clay colloids before injection through columns packed with geologic media to provide estimates of desorption rate constants (from colloids) and other parameters that are important for performance assessment calculations. While our studies focused on a specific crystalline rock system, the method(s) we developed can, in principle, be applied to any geologic setting in which colloid-facilitated transport in groundwater is a potential mechanism for radionuclide release to the accessible environment. The methods are intended to especially provide insights into upscaling of colloid-facilitated radionuclide transport predictions in time and space.

For this study, we selected a fractured/weathered granodiorite at the Grimsel Test Site (GTS) in Switzerland as a model crystalline rock repository system because the system has been thoroughly studied (e.g., Dittrich and Reimus, 2013; Geckeis et al., 2004; Huber et al., 2011; Wang et al., 2013b), and field experiments involving radionuclides have already been conducted at this site (Geckeis et al., 2004; Möri, 2004; Wang et al., 2013a; Dittrich et al.., 2014). Working on this system provides a unique opportunity to compare lab experimental results with field-scale observations.

Field experiments and observations in a shear zone at the GTS have shown that Cs transport in a fractured crystalline environment can be enhanced by the presence of bentonite colloids (Geckeis et al., 2004; Möri, 2004; Wang et al., 2013a). In an experiment conducted at the GTS in 2002 as part of the a Colloid and Radionuclide Retardation (CRR) project, a significant fraction (~60%) of ^{137}Cs associated with colloids transported essentially conservatively in a dipole tracer test conducted between two boreholes completed in the shear zone. The mean conservative tracer residence time in this experiment was on the order of 2 hours, with peak tracer concentrations occurring in about 70 minutes. Interestingly, a second peak of ^{137}Cs, accounting for less than 10% of the injected mass, was observed at about 100 times longer than the first peak. This peak likely reflected the retardation of dissolved ^{137}Cs that was not associated with the colloids (or had become dissociated from the colloids during transport through the shear zone), as the colloid concentrations had essentially declined to background long before this peak was observed (Geckeis et al., 2004; Möri, 2004). In 2012, a second colloid-facilitated transport experiment involving ^{137}Cs was conducted at the GTS under the Colloids Formation and Migration (CFM) project (Wang et al., 2013a). This experiment was conducted in a different dipole than the 2002 test (between a borehole and the access tunnel wall) and with a mean residence time of about 34 hours. In this experiment, the ^{137}Cs recovery was only about 10% and the breakthrough curve closely matched the shape of the bentonite colloid breakthrough curve, indicating that the observed ^{137}Cs was essentially all associated with the colloids. A second ^{137}Cs peak was not observed in this experiment, although this may have been because the experiment was not conducted long enough to observe such a peak. A second peak would have taken about a year to arrive if the delay relative to the first peak was the same as in the 2002 experiment.

Laboratory experiments to evaluate the association of Cs with bentonite or smectite colloids have been conducted by several research groups (Murali and Mathur, 2002; Missana et al., 2004; Geckeis et al., 2004; Kurosawa et al., 2004; Iijima et al., 2010). The experiments of Missana et al. (2004), Geckeis et al.

(2004) and Iijima et al. (2010) focused on the Grimsel system, although the bentonite colloids used by Iijima et al. (2010) were derived from a different bentonite source. These experiments, and in particular the work of Missana et al. (2004), have shown that Cs sorption to GTS bentonite colloids has a nonlinear dependence on Cs concentrations and that desorption of at least a portion of the sorbed Cs is slow and potentially incomplete (partial sorption irreversibility). The dependence of Cs partition coefficients (K_d values) onto the bentonite colloids as a function of Cs concentration measured by Missana et al. (2004) is reproduced in Figure 7-1. In general, the work of the other research groups mentioned above are in reasonable agreement with Missana et al. (2004) when the Cs concentrations in the respective experiments are considered.

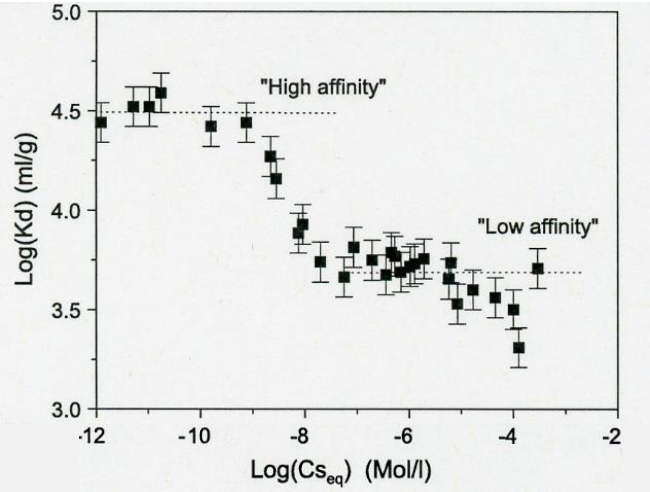

Figure 7-1. Batch adsorption K_d values for ^{137}Cs on same bentonite colloids as used in this study in GTS groundwater as a function of Cs concentration (reproduced from Missana et al., 2004).

In this study, we conducted both batch and column transport experiments to refine and parameterize a colloid-facilitated transport model and to provide insight into potential colloid-facilitated transport of Cs isotopes in a crystalline rock repository. The batch experiments included both Cs adsorption and desorption experiments onto fracture fill material (FFM) obtained from the GTS shear zone. We also measured the partitioning of Cs onto colloids that were prepared from the same bentonite that was used in the GTS field experiments (also the same bentonite used by Missana et al., 2004). The starting concentration of Cs in these experiments was not varied, but rather was kept the same as the injection solutions for the column experiments so that we could compare the batch test parameters with parameters derived from the column experiments. Column experiments were conducted with (1) Cs injected without colloids, (2) Cs injected pre-sorbed onto colloids with the colloid pulse ending at the same time as the Cs pulse, and (3) Cs injected pre-sorbed onto colloids with the colloids continuously fed through the column after the Cs pulse had ended.

An update of work conducted for the Colloids Formation and Migration Project at the Grimsel Test Site is not included in this report other than to say that the majority of the work over the past 1-1/2 years has involved the emplacement and subsequent long-term monitoring of a radionuclide-doped bentonite plug into a borehole at the GTS that intersects the flowing shear zone in which previous colloid-facilitated radionuclide transport experiments were conducted. The emplacement of the doped bentonite was accomplished in May 2014, and since then monitoring has indicated that the bentonite rapidly (within about 2 weeks) swelled to fill and pressurize the emplacement interval (between two packers instrumented with pressure sensors) and that a small amount of the conservative dye tracer included with the doped bentonite has appeared at both a near-field monitoring borehole (located several cm from the main emplacement hole) and at the access tunnel wall where a surface packer is being used as a controlled

hydrologic sink. It also appears that the near-field monitoring borehole is registering a slight increase in groundwater turbidity, which suggests the appearance of colloids eroding from the bentonite plug. These results are all very preliminary, and as a courtesy to the CFM project participants, it would not be appropriate to present them in written form for the first time in this report.

7.2 State of the Art

The current state of the art in conducting colloid-facilitated contaminant/radionuclide transport experiments and in modeling colloid-facilitated transport has been addressed at length in the literature. Excellent reviews are provided by Grolimund et al. (2007), Bertetti et al. (2006), Kanti and Khilar (2006), Grolimund and Borkovec (2005), Painter et al., (2002), and Kersting and Reimus (2003). These reviews cite many earlier efforts. Modeling of colloid-facilitated contaminant transport has progressed very little in the past 20 years, but incremental advances have been made in parameterizing models and reducing uncertainty in model predictions by designing and conducting experiments that better interrogate the processes that result in colloid-facilitated transport over long time and distance scales (i.e., slow desorption colloids and slow or reversible colloid filtration). For example, in Dittrich et al. (2015a; 2014), we introduced a method of reinjecting effluent from colloid-facilitated radionuclide transport column experiments into subsequent columns to allow better interrogation of slow desorption kinetics from colloids, which are very important for predicting colloid-facilitated transport in upscaled systems. In this study, we build on that approach and apply it to a study of the colloid-facilitated transport of Cs.

7.3 Technical Approaches (Materials and Methods)

We conducted a series of batch adsorption and desorption experiments, as well as three flow-through experiments in small columns to evaluate the colloid-facilitated transport of Cs in the shear zone at the GTS. The materials and methods are described in this section.

7.3.1 Groundwater

The groundwater used in all experiments was synthetic shear zone water (SZW) that matched the water chemistry of the water in the shear zone at the Grimsel Test Site. The SZW was prepared by adding analytical grade reagents to filtered, high-purity water (> 18 MΩ cm resistivity) according to the concentrations of constituents listed in Table 7-1.

The ionic strength (0.66 mM) was calculated from the added reagents and a pH of 8.0 was measured the solution equilibrated with the atmosphere in Los Alamos, NM (2,231 m above sea level). The carbonate concentration listed in Table 3-1 is as prepared, not after equilibration with the atmosphere.

Table 7-1. Synthetic shear zone water constituents.

Constituent	mg/L
Na	14.97
K	0.20
Mg	0.02
Ca	5.60
Cl	5.67
SO_4	5.85
F	6.00
Si	9.96
CO_3+HCO_3	20.06
Ionic Strength	0.66 mM
pH	8.0

7.3.2 Geologic Media

Weathered fracture fill material, or FFM (also known as fault gouge), was collected by coring the MI shear zone at the Grimsel Test Site (GTS) in Switzerland. The shear zone is not currently exposed in the CFM tunnel (where the field transport experiments were conducted), so the material was collected in an adjacent tunnel. The shear zone occurs where a fracture in the granite rock had been exposed to hydrothermal solutions and was altered over time. Samples were shipped to Los Alamos National Laboratory in pieces ranging from micron size up to 10-15 cm long. Due to the small quantity of material available, all pieces less than 1 cm in size were combined and crushed using a percussion mortar, sieved into 75-150, 150-355, and 355-500 µm size fractions, and thoroughly rinsed in high-purity water to removal all fines. The samples were then rinsed with synthetic Grimsel shear zone water (SZW) until the electrical conductivity of solution in contact with the material for 24 hours was within 5% of the electrical conductivity of the SZW. Samples were then oven dried for 12 hours at 60 °C and stored in glass jars. Optical microscope (Wild Heerbrugg, M420) photographs of the 150-355 µm size fraction of the FFM and the unaltered granodiorite matrix show that the FFM appears to have a larger fraction of dark grains (Figure 7-2).

The mineralogy of the granodiorite and FFM were determined by quantitative x-ray diffraction (QXRD) at Los Alamos. Table 7-2 lists the major fractions for the unaltered granodiorite, a scraping from the shear zone surface and a bulk sample of the crushed FFM that we used for all experiments discussed in this report.

Table 7-3 shows the bulk chemical analysis of the granodiorite and bulk FFM by x-ray florescence spectroscopy. The main differences between the unaltered granodiorite and FFM were a significant

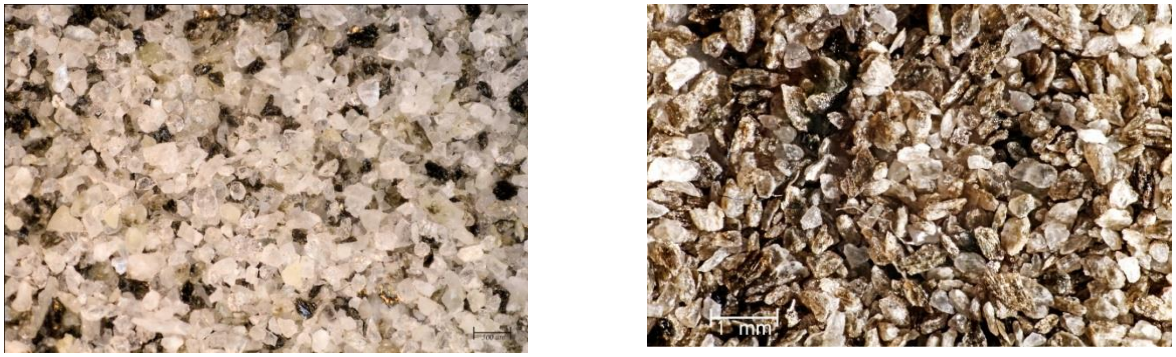

Figure 7-2. Microphotographs of crushed and sieved Grimsel granodiorite (left) and fracture fill material (right) in the 150-355 µm size fraction (from Dittrich and Reimus, 2015 and Dittrich et al., 2015a).

Table 7-2. Quantitative X-ray diffraction interpretation (wt%) of Grimsel granodiorite, shear zone surface, and bulk FFM materials.

Mineral	Granodiorite	Shear Zone Surface	FFM
Quartz	32	18	13
Microcline	10	8	5
Albite	42	44	34
Biotite	5	11	31
Chlorite	1	--	
Muscovite	10	19	16
Epidote	<1	--	--
Smectite	--	--	1

Table 7-3. Bulk chemical analysis of granodiorite and FFM materials by X-ray fluorescence analysis (wt%).

Constituent	Granodiorite bulk	FFM bulk	Detection Limits
fuse ratio	7:1	7:1	7:1
Na_2O	4.01	3.15	0.0451
MgO	0.725	4.28	0.0300
$Al2O_3$	14.0	14.3	0.0313
SiO_2	70.9	63.4	0.1507
P_2O_5	0.115	0.124	0.0049
K_2O	4.22	4.90	0.0112
CaO	1.90	1.03	0.0084
TiO_2	0.436	0.491	0.0092
MnO	0.081	0.086	0.0252
$Fe2O_3$	3.10	3.83	0.0041
V	29	41	13
Cr	bdl	bdl	10
Co	bdl	bdl	15
Ni	bdl	bdl	5
Cu	bdl	bdl	5
Zn	31	53	5
Ge	bdl	bdl	24
As	bdl	bdl	15
Rb	110	192	4
Sr	135	71	5
Zr	217	236	6
Ba	403	372	19
W	bdl	bdl	43
U	bdl	bdl	4
LOI	0.35	4.28	
total	99.931	99.970	

bdl = below detection limit
LOI = loss on ignition

enrichment in Mg, minor enrichment in K and Fe, and minor depletions of Si, Na, and Ca in the FFM relative to the parent granodiorite.

The surface area of the FFM was determined by the BET method with krypton gas (Micromeritics Analytical Services) and was measured as 0.23 $m^2\ g^{-1}$ for the 150-355 μm size fraction used in all experiments.

7.3.3 Bentonite Colloids

Bentonite colloids were processed from a brick of compressed bentonite from the Corijo de Archidona deposit (Almeria, Spain) that was shipped to us by our colleagues from the Grimsel Test Site in Switzerland. This material is also called FEBEX bentonite because it was used in the Full-scale high-level waste Engineered Barriers EXperiment at the GTS, which goes by the acronym FEBEX. The major mineralogy of this bentonite, as determined by quantitative XRD by our European colleagues, is given in Table 7-4. Samples of the brick were crushed in a ceramic mortar and pestle and sieved to retain the size fraction less than 75 µm. The bentonite colloids were sodium saturated to enable comparison of our results with other published results (Huber et al., 2011). 50 g of material was added to 1 L of 1 M NaCl and was placed on a shaker table for 7 days. The supernatant was decanted and the removed liquid was replaced with new 1 M NaCl and placed on the shaker for 7 additional days. This process was repeated 3 times and the solution conductivity was measured (VWR Series 500, Model 2052 meter and VWR 525 conductivity dip cell/electrode, Model 23198-020) to ensure completeness of the exchange process. The resulting suspension was settled and the supernatant was decanted and replaced with SZW. This process was repeated 6 times until the conductivity of the supernatant was reduced below 2.5 mS/cm and the colloids did not readily settle. The suspension was then placed in a sonic bath for 30 min, centrifuged for 12 hr, and the supernatant removed and replaced with SZW. This process was repeated 10 times until the resulting conductivity of the bentonite suspension was within 1% of the SZW. Various steps of the process are depicted in Figure 7-3.

The suspension was then diluted to 1 g L^{-1} with SZW and was settled in 1 L graduated cylinders for 2 weeks to obtain a stable experimental suspension. The top 700 mL was decanted and Stokes' Law was applied to calculate a theoretical maximum particle size of less than 1 µm. The final stock suspension was then passed through a 0.8 µm filter to remove any larger particles. A single particle counter was used to measure the particle size distribution of the stock suspension. Very few particles larger than 220 µm were present (Figure 7-4).

The concentration of the stock suspension was calculated to be (1540 mg L^{-1}) by drying 25 mL of suspension on a watch glass (in triplicate) and determining the weight difference after drying. The stock suspension was diluted to 100 mg L^{-1} and was stored in a sealed glass bottle. Surface area of the dried colloids was measured by the BET method with nitrogen gas to be 56.1 m^2 g^{-1}.

Table 7-4. Quantitative X-ray diffraction interpretation (wt%) of FEBEX bentonite.

Mineral	Bentonite
Quartz	2 ± 1
Plagioclase (Na, Ca)	3 ± 1
Cristobalite	2 ± 1
Feldspars	Trace
Smectite	92 ± 3
Calcite	1 ± 0.5

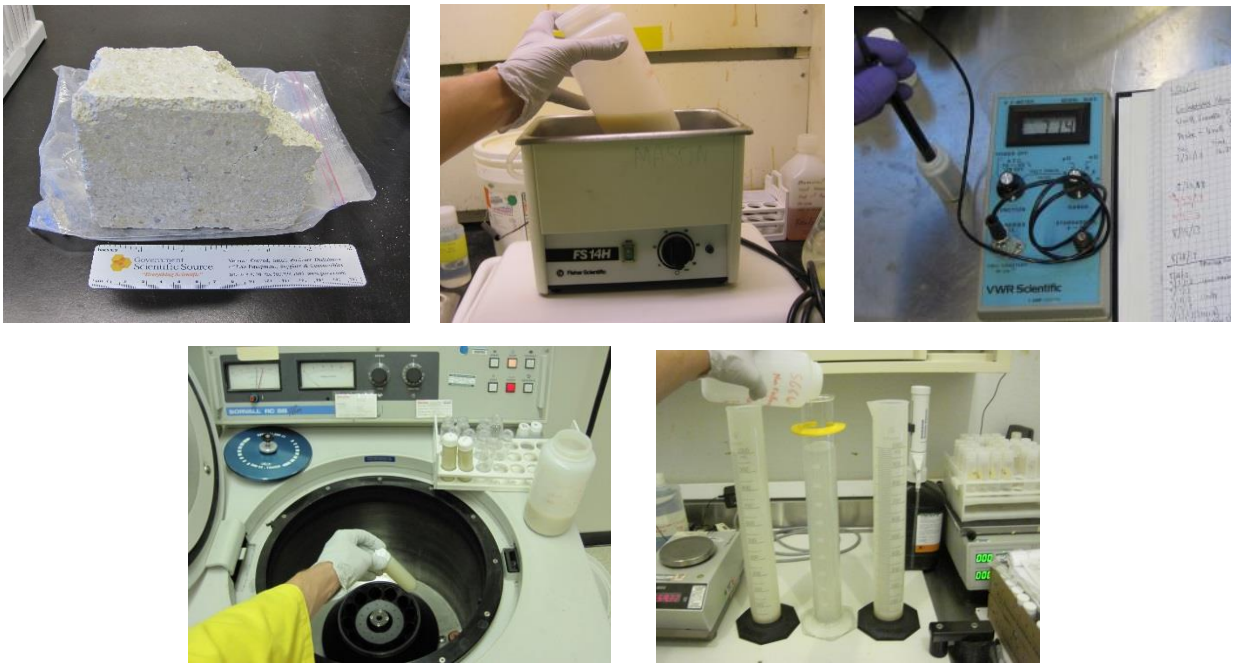

Figure 7-3. Various steps in preparation of colloid suspension from FEBEX bentonite brick.

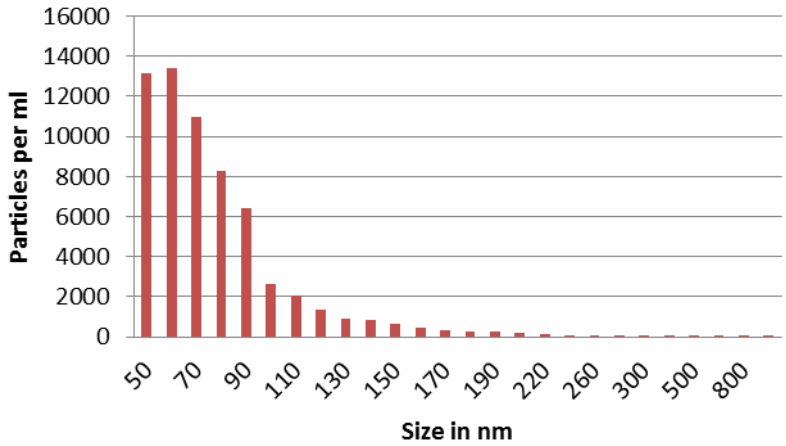

Figure 7-4. Particle size distribution of FEBEX bentonite colloid suspension as measured by a single particle counter. Note that the concentration scale on the y-axis does not account for sample dilution in the final suspension used in the experiments.

7.3.4 Cesium and Tritiated Water

The Cs used in all experiments was taken from a ^{137}CsCl stock in 0.1 M HCl (Eckert and Ziegler). The stock solution contained 3.056 μCi of ^{137}Cs (referenced to 10/1/2011) in 100 ml of aqueous solution, corresponding to a concentration of 2.6e-9 M ^{137}Cs. The solution contained 10 μg/ml, or 7.5e-5 M, of carrier (nonradioactive) Cs. When the SZW with 100 mg/L of suspended bentonite colloids was initially spiked with a small amount of this solution, NaOH was added to the suspension to neutralize the HCl from the stock solution and re-establish the pH of 8. This NaOH addition resulted in exceeding the ionic strength threshold for colloid stability, which led to colloid aggregation and settling to the bottom of the container. The colloids were resuspended by decanting off most of the supernatant and adding enough

fresh SZW to re-establish the 100 mg/L colloid concentration (and also to re-establish the unaltered or only slightly-altered Na and Cl concentrations in the SZW). The resulting solution was sonicated to re-disperse the colloids, and after sonication and settling, the colloid size distribution was found to be essentially indistinguishable from the original size distribution shown in Figure 7-4. After this procedure, the ^{137}Cs concentration in the suspension was about 3e-11 M, and the total Cs concentration was inferred to be ~9e-7 M. This process was repeated for subsequent batches of Cs-spiked colloid suspensions. The suspensions were allowed to equilibrate for at least 1 week. All suspensions were stored in Teflon® bottles until used in experiments.

Tritium in the form of tritiated water (^{3}HHO) was added to the Cs and bentonite suspensions and was used as a conservative tracer to provide groundwater residence times and dispersivities in the column experiments.

7.3.5 Analytical Measurements

^{137}Cs and tritium concentrations were measured by liquid scintillation counting, or LSC (Perkin Elmer Tri-Carb 2550) with energy ranges of 0-15 keV for tritium and 15-225 keV for ^{137}Cs (energies uncorrected for quenching). A 1 mL aliquot of sample was combined with 5 mL of deionized water and 14 mL of liquid scintillation cocktail (Packard, Ultima Gold AB) in a polypropylene scintillation vial to yield 20 mL total. The vial was vigorously shaken for at least 15 seconds to ensure mixing between the cocktail and the sample, and samples were counted for two 15 minute increments and the results were averaged. The transformed index of an external ^{133}Ba standard (tSIE) was used to correct for variable quenching of the samples, especially with respect to tritium.

Total ^{137}Cs concentrations were measured with uncentrifuged column effluent and dissolved ^{137}Cs was measured by centrifuging the sample at 15,000 RPM for 12 hours and then analyzing 1 mL of the supernatant for ^{137}Cs concentration. Colloid-associated ^{137}Cs was then calculated as the difference between the total and dissolved ^{137}Cs concentration for each sample.

pH of the solutions, suspensions, and breakthrough experiment samples were measured using a pH meter (Orion, Model 290) and a glass pH electrode (Fisher, AccupHast) calibrated with 4.01, 7.00, and 9.01 pH buffer solutions (Ricca Chemical Corp.).

Colloid concentrations of the bentonite suspensions in the column breakthrough experiments were measured using turbidimetry. The turbidimeter (Hach, 2100N) was calibrated with standards (0.1, 1, 5, 10, 20, 40, 60, 80, 100 mg L^{-1}) and the same 12 mm borosilicate glass test tube was used for every measurement to reduce error from test tube variability. Colloid concentrations were calculated using a correlation function derived to relate colloid concentration with the measured NTU (nephelometric turbidity units) of the samples.

7.3.6 Batch Experiments

Batch adsorption and desorption experiments were conducted to evaluate the interaction of Cs with crushed FFM that was used in the column experiments. The experiments were performed in duplicate in polycarbonate centrifuge tubes, and a control experiment without the FFM was also conducted to allow corrections for any interaction of the Cs with the centrifuge tube walls. All sorption experiments were conducted using colloid-free SZW spiked with ^{137}Cs to the same concentration as in the colloid suspensions (with appropriate dilution with SZW to match the Na and Cl concentrations; see Section 7.3.4). In the reactors containing FFM, 20 ml of ^{137}Cs-spiked colloid-free SZW was placed in contact with 0.25 g of the FFM. The sorption experiments were conducted for ~70 hours, with samples collected from the centrifuge tubes after 2.5 and 30 min, and also after 3.1, 5.25, 20.3, 40.6 and 68.9 hr. All but approximately 1 ml of the remaining solution was then decanted off, and 20 ml of ^{137}Cs-free SZW was added to start duplicate desorption experiments (with a control as well). In the desorption experiments, samples were collected after 1, 7, 22 and 48 min, and also after 3.7, 6.1, 21.5, 46.1 and 70 hrs. All but 1 ml of the remaining solution was then again decanted off and 20 ml of ^{137}Cs-free SZW was added to start

a second desorption step/experiment. However, for this step, one of the centrifuge tubes containing FFM received SZW that contained suspended colloids at 100 mg/L while the other received colloid-free SZW. In these desorption experiments, samples were collected after 1, 10, 20, 45, 70 min, and also after 3.6, 5.75, 21.4, 28.6, 48.5, 76 and 142 hrs.

Formal sorption and desorption experiments were not conducted to evaluate ^{137}Cs partitioning between the bentonite colloids and the SZW, but this partitioning was measured numerous times throughout the course of the study, and the ^{137}Cs was consistently found to be about 23-25% associated with the colloids and 75-77% in the solution phase. This result translates to a partition coefficient, or K_d value, of approximately 3700 ml/g, which is consistent with the results of Missana et al. (2004) for concentrations exceeding about 1e-8 M Cs (see Figure 7-1).

7.3.7 Column Transport Experiments

Column transport experiments were conducted by eluting Cs and bentonite suspensions through columns packed with FFM in the 150-355 μm size range. Small columns were constructed from 1.5 cm lengths of 0.95 cm diameter Teflon® tubing (Dittrich et al., 2015b). The ends of the tubes were tapped to accept Teflon® compression fittings. The inside openings were covered with a small disk of 75 μm PEEK screen to retain the column material while providing minimum resistance to flow and causing negligible straining of colloids. Teflon® tubing (1/16th-inch ID) and 3-way polycarbonate stopcocks were used to connect the columns to 60 mL polypropylene syringes (Becton Dickinson) installed on syringe pumps (KD Scientific, Model 100). 3-way stopcocks allowed for refilling syringes and switching suspensions or solutions while minimizing flow and pressure disturbances that may affect colloid retention. Flow was directed upward to help maintain saturation and to minimize the potential for air bubbles collecting in the columns. An additional length of 1/16th-inch ID Teflon® tubing was connected to the top (outlet side) of the column and directed column effluent to a fraction collector (Gilson, FC-220) filled with 13 × 100 mm polystyrene test tubes. The fraction collector was enclosed in an acrylic plastic chamber with evaporation pans filled with deionized water to minimize evaporation before sample analysis. Figure 7-5 shows a picture of the column experiment setup.

Columns were packed with 1.5 g of dry FFM, resulting in a porosity of approximately 0.4 and a bulk density of about 1.6 g/cm^3. The columns were initially flushed at ~0.3 ml/hr with ^{137}Cs-, ^{3}HHO-, and colloid-free SZW for 7 days and the pH was monitored to ensure effluent pH stabilized within 0.1 pH units of the influent solution (pH 8.0 ± 0.1) before the start of a radionuclide/colloid injection.

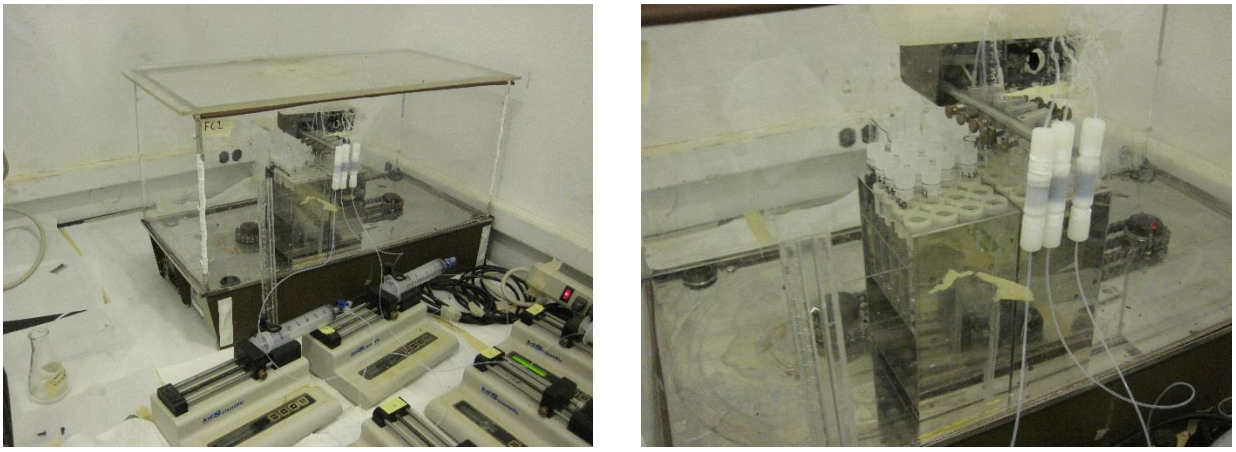

Figure 7-5. Photos of column experiment setup with three 1.5-cm-long columns running in parallel with syringe pumps, tubing, and fraction collector.

To begin each breakthrough experiment, the background solution was switched to either a bentonite suspension in SZW (100 mg/L bentonite) that contained ^{3}HHO and ^{137}Cs (3e-11 M ^{137}Cs, 9e-7 M total Cs, see Section 7.3.4) or to colloid-free SZW containing the same concentrations of ^{3}HHO and ^{137}Cs. Two identical columns were used; one received the ^{137}Cs-spiked colloid suspension and the other received the colloid-free spiked solution. The flow rates through the columns were nominally ~0.28 ml/hr. Syringes were refilled several times during the experiment and were eventually changed to SZW free of ^{3}HHO, ^{137}Cs, and bentonite colloids to observe the flushing of the colloids and ^{137}Cs from the columns. Samples were collected at 12 hr intervals and the sample mass was weighed with a digital balance (Mettler, PL1200) and subtracted from the empty test tube weight to calculate the actual flow rates. Total and dissolved ^{137}Cs activity, tritium activity, and colloid concentrations were measured (see Section 7.3.5) for every sample early in the breakthroughs and then less often as the experiments progressed.

Once the ^{137}Cs concentration in the effluent from the column injected with the colloid suspension reached the inlet ^{137}Cs concentration, the effluent that wasn't used for radionuclide or colloid analyses was stored in a Teflon® bottle for re-use. This combined effluent was then injected into another FFM-filled column that had not been previously exposed to colloids or ^{137}Cs. The same procedure was followed as the other two columns except that after the injection solution was exhausted, the solution in the syringes was changed to ^{3}HHO- and ^{137}Cs-free SZW that contained suspended colloids at the same concentration as the combined effluent injected at the beginning of the experiment. Thus, while the injection of ^{3}HHO and Cs ceased, the injection of colloids continued without interruption for the remainder of the experiment.

At the end of each column experiment, a 0.1 M HCl solution was flushed through the column to desorb any ^{137}Cs remaining in the column and attempt to close the Cs mass balance for the experiment.

Control column experiments containing no FFM but with all the other experimental components were also conducted to evaluate interaction of Cs with any of the components other than the FFM, and it was found that interactions were negligible, so the results of these experiments are not presented in this report.

7.3.8 Interpretive Modeling

The batch experiments were interpreted by simply calculating ^{137}Cs partition coefficients near the end of the experiments for either adsorption or desorption. The partition coefficients were calculated as:

Adsorption: $$K_d = \frac{V}{M}\frac{(C_0 - C)}{C} \quad (7\text{-}1)$$

Desorption: $$K_d = \frac{V_{des}}{M}\frac{[(C_0 - C)_{ads}V_{ads} + C_{ads}V_{res,ads} - CV_{des}]}{CV_{des}} \text{ or } K_d = \frac{V_{des}}{M}\frac{S}{C} \quad (7\text{-}2)$$

where, V = volume of solution, ml
M = mass of FFM or colloids, g
C = concentration at end of experiment, mol/ml
C_0 = concentration at beginning of experiment, mol/ml
S = concentration on FFM or colloids, mol/g (calculated using data from previous step)
ads = subscript for adsorption step
des = subscript for desorption step
$V_{res,ads}$ = volume of residual solution remaining behind after adsorption step, ml

The adsorption and desorption rate constants were not estimated from the batch experiments because the rates were observed to be very rapid – so much so that they were thought to be potentially limited by mass transfer rates in the batch reactors, especially considering the large volume to solid mass ratios in the centrifuge tubes. Also, when sorption site capacities are allowed to vary, estimates of rate constants from batch experiments are notoriously nonunique (a smaller site capacity and faster rate constants will often yield equally good fits to a data set as a larger site capacity and smaller rate constants). Thus, rather than

attempt to estimate rate constants from the batch experiments, the rate constants were estimated by interpreting the column experiment data, and then the rates deduced from the columns were used to do a forward prediction of the batch sorption/desorption experiments. The forward batch experiment model was embodied in a Fortran program that allowed multiple sites with different rate constants and adsorption capacities (Dittrich et al., 2014). The governing equations of the model were:

$$\text{Solution:} \quad \frac{\partial c}{\partial t} = \frac{M}{V}\left[-\sum_i k_{fi} c \left(1 - \frac{s_i}{s_{mi}}\right) + \sum_i k_{ri} s_i\right] \tag{7-3}$$

$$\text{Solids:} \quad \frac{\partial s_i}{\partial t} = k_{fi} c \left(1 - \frac{s_i}{s_{mi}}\right) - k_{ri} s_i \tag{7-4}$$

where, c = concentration in aqueous phase, mol/ml
s_i = concentration on surface sorption site i, mol/g
t = time, hr
k_{fi} = adsorption rate constant for sorption site i, ml/g-hr
k_{ri} = desorption rate constant for site i, hr^{-1}
s_{mi} = surface site density (maximum adsorption capacity) for sorption site i, mol/g
M = mass of solids, g
V = volume of solution, ml.

In addition to solving equations (3) and (4), the batch model allowed the volume of solution in the reactor to be changed at specified times to simulate sampling, and it also allowed for a specified volume of Cs-free water to be added to the reactor to simulate the start of the desorption phase of the experiments. Equations (3) and (4) were solved using a 4th-order Runge-Kutta algorithm.

The model used to interpret the column transport experiments was also embodied in a Fortran program that was described previously in Dittrich et al. (2014). Although the model allows for dual-porosity transport (including diffusion into a stagnant secondary porosity that has sorption properties), it was found that the model matches to the column breakthrough curves were not improved by including a secondary porosity, so the secondary porosity features of the model are not described below.

Colloid Transport in Flowing Porosity:

$$\text{Mobile:} \quad \frac{\partial C_{col}}{\partial t} + v_f \frac{\partial C_{col}}{\partial x} - D_c \frac{\partial^2 C_{col}}{\partial x^2} + k_{fc} C_{col} - k_{rc} S_{col} + k_{fci} C_{col} - P_{col} = 0 \tag{7-5}$$

$$\text{Immobile:} \quad \frac{\partial S_{col}}{\partial t} - k_{fc} C_{col} + k_{rc} S_{col} - k_{fci} C_{col} = 0 \tag{7-6}$$

Solute Transport in Flowing Porosity:

$$\begin{aligned} &\frac{\partial C}{\partial t} + v_f \frac{\partial C}{\partial x} - D_f \frac{\partial^2 C}{\partial x^2} + k_{1f} C C_{col}\left(1 - \frac{C_1}{C_{col} S_1^0}\right) + k_{2f} C\, C_{col}\left(1 - \frac{C_2}{C_{col} S_2^0}\right) + \\ &\left(\frac{\rho_f}{\eta}\right)\left[\sum_i k_{fi} C\left(1 - \frac{S_i}{S_{mi}}\right) - \sum_i k_{ri} S_i\right] + k_{1f} C S_{col}\left(1 - \frac{C_{filt,1}}{S_{col} S_1^0}\right) + k_{2f} C S_{col}\left(1 - \frac{C_{filt,2}}{S_{col} S_2^0}\right) - \\ &k_{1b} C_1 - k_{2r} C_2 - k_{1b} C_{filt,1} - k_{2r} C_{filt,2} = 0 \end{aligned} \tag{7-7}$$

Solute Transport on mobile colloids while adsorbed to colloid sites 1 and 2:

$$\frac{\partial C_1}{\partial t} + v_f \frac{\partial C_1}{\partial x} - D_c \frac{\partial^2 C_1}{\partial x^2} - k_{1f} C C_{col} \left(1 - \frac{C_1}{C_{col} S_1^0}\right) - k_{rc} C_{filt,1} + k_{1r} C_1 + k_{fc} C_1 - P_{col} S_a = 0 \quad (7\text{-}8)$$

$$\frac{\partial C_2}{\partial t} + v_f \frac{\partial C_2}{\partial x} - D_c \frac{\partial^2 C_2}{\partial x^2} - k_{2f} C C_{col} \left(1 - \frac{C_2}{C_{col} S_2^0}\right) - k_{rc} C_{filt,2} + k_{2r} C_2 + k_{fc} C_2 - P_{col} S_b = 0 \quad (7\text{-}9)$$

Immobile Solute in Fractures (sorption sites a and b):

$$\frac{\partial S_i}{\partial t} - \sum_i k_{fi} C \left(1 - \frac{S_i}{S_{mi}}\right) + \sum_i k_{ri} S_i = 0 \quad (7\text{-}10)$$

Immobile Solute adorbed onto Immobile Colloids in Fractures (colloid sites 1 and 2):

$$\frac{\partial C_{filt,1}}{\partial t} - k_{1f} C S_{col} \left(1 - \frac{C_{filt,1}}{S_{col} S_1^0}\right) - (k_{fc} + k_{fci}) C_1 + k_{rc} C_{filt,1} + k_{1r} C_{filt,1} = 0 \quad (7\text{-}11)$$

$$\frac{\partial C_{filt,2}}{\partial t} - k_{2f} C S_{col} \left(1 - \frac{C_{filt,2}}{S_{col} S_2^0}\right) - (k_{fc} + k_{fci}) C_2 + k_{rc} C_{filt,2} + k_{2r} C_{filt,2} = 0 \quad (7\text{-}12)$$

where, C_{col} = concentration of colloids in solute phase, mol/cm^3
S_{col} = colloid concentration on media surfaces, mol/cm^3
C = solution concentration of solute in flowing porosity, mol/cm^3
S_i = sorbed concentration of solute on media surface site *i*, mol/g
C_1 = concentration of solute sorbed to site 1 on mobile colloids, mol/cm^3
C_2 = concentration of solute sorbed to site 2 on mobile colloids, mol/cm^3
$C_{filt,1}$ = concentration of solute sorbed to site 1 on immobile colloids, mol/cm^3
$C_{filt,2}$ = concentration of solute sorbed to site 2 on immobile colloids, mol/cm^3
P_{col} = colloid production rate in flowing porosity, g/cm^3-hr
v_f = fluid velocity in flowing porosity, cm/hr
D_f = solute dispersion coefficient in flowing porosity, cm^2/hr
D_c = colloid dispersion coefficient in flowing porosity, cm^2/hr
ρ_f = effective bulk density within flowing porosity, g/cm^3
η = porosity in flow domain
k_{fc} = colloid filtration rate constant (1/hr) = λv_f, where λ = filtration coefficient (1/cm)
k_{rc} = reverse colloid filtration (detachment) rate constant, 1/hr
k_{fci} = irreversible colloid filtration rate constant, 1/hr
k_{fi} = rate constant for sorption of solute onto media surface site *i*, ml/g-hr
k_{ri} = rate constant for desorption of solute from media surface site *i*, 1/hr
k_{1f} = rate constant for sorption of solute onto colloid surface site 1, ml/g-hr
k_{1r} = rate constant for desorption of solute from colloid surface site 1, 1/hr
k_{2f} = rate constant for sorption of solute onto colloid surface site 2, ml/g-hr
k_{2r} = rate constant for desorption of solute from colloid surface site 2, 1/hr
S_1^0 = maximum solute capacity on colloid sorption site 1, mol/g colloid
S_2^0 = maximum solute capacity on colloid sorption site 2, mol/g colloid
S_{mi} = maximum solute capacity on media sorption site *i*, mol/g solid

The model allows for up to 5 different types of sorption sites, with different rate constants and sorption capacities, to be specified on the immobile media surfaces (the FFM), but it only allows for 2 different types of sorption sites on the colloids. Both reversible and irreversible colloid filtration can be simulated, although the bentonite colloids in this study transported essentially conservatively through the 1.5-cm columns, so the filtration rate constants were set to zero and filtration was effectively ignored.

The column modeling procedure involved first using the ^{3}HHO breakthrough curves to obtain estimates of the mean residence time and dispersivity in the columns, and then these parameters were assumed to apply to the transport of colloids and Cs through the columns. Rapid and reversible adsorption of the Cs onto the colloids was assumed based on observations that the Cs partitioning to the colloids occurred as rapidly as could be measured when ^{137}Cs-spiked suspensions were prepared. The ratios of adsorption rate constants to desorption rate constants for the Cs on both the colloids and the FFM were constrained by the partitioning observed in the batch experiments, but the rate constants themselves were allowed to vary to match the observed breakthrough curves. Further details of the procedure are provided in the next section.

7.4 Technical Results

7.4.1 Batch Experiment Results

The results of batch adsorption experiments of the Cs onto the FFM are shown in Figure 7-6. The duplicate FFM experiments are in excellent agreement, and the control experiment shows no evidence of any interaction of Cs with the centrifuge tubes. The partition coefficient, or K_d value, at the end of the experiment is calculated (eq. 7-1) to be approximately 51 ml/g. This value is much lower than the K_d value of ~3600 ml/g calculated for Cs partitioning to the bentonite colloids, but when one considers the much larger specific surface area of the colloids vs. the FFM (56.1 m^2/g vs. 0.23 m^2/g), the Cs partition coefficient on a surface area basis is actually slightly larger for the FFM than for the colloids: 220 ml/m^2 for the FFM vs. 64 ml/m^2 for the colloids. The model curves shown in Figure 7-6 were generated using the batch adsorption model described in Section 7.3.8 with the sorption and desorption rate constants that provided the best matches to the column data (see Section 7.4.2), so they were not optimized to offer the best fits to the batch data. It is apparent that the parameters yielding a good match to the column data also provided reasonably good matches to the batch data, particularly in the case of the two-site model.

The results of the two desorption experiments evaluating Cs desorption from the FFM are shown in Figures 7-7 and 7-8, respectively. Figure 7-7 shows that the duplicate experiments are again in excellent agreement. The K_d value at the end of this experiment is calculated (eq. 7-2) to be approximately 200 ml/g, or nearly 4 times greater than the K_d value at the end of the adsorption experiment. This result indicates that there is some adsorption-desorption hysteresis, with at least a portion of the adsorbed Cs not readily desorbing from the FFM or desorbing at a slower rate than the remainder of the Cs. This result might also be interpreted as an indication of a nonlinear adsorption isotherm, as the Cs concentration in solution at the end of the desorption experiment is about a factor of 5.5 lower than at the end of the adsorption experiment. Either way, it appears that Cs was desorbed preferentially from weaker sorption sites and the Cs remaining on the FFM after desorption is, on average, more strongly associated with the FFM than the Cs at the end of the adsorption experiment. As in the case of Figure 7-6, the model curves in Figure 7-7 show the desorption of Cs from the FFM predicted using the model parameters that provided good matches to the column transport data (see Section 7.4.2). They are not optimized fits to the batch desorption data.

In Figure 7-8, there is a difference between the two desorption curves because the desorption solution added to one of the centrifuge tubes included Cs-free bentonite colloids at ~100 mg/L while the other solution was colloid-free SZW. The data points for the experiment with colloids are measurements of samples that were not centrifuged to remove the colloidal fraction of Cs, so these data represent dissolved plus colloidal Cs concentrations. It is apparent that more of the Cs desorbed from the FFM when the

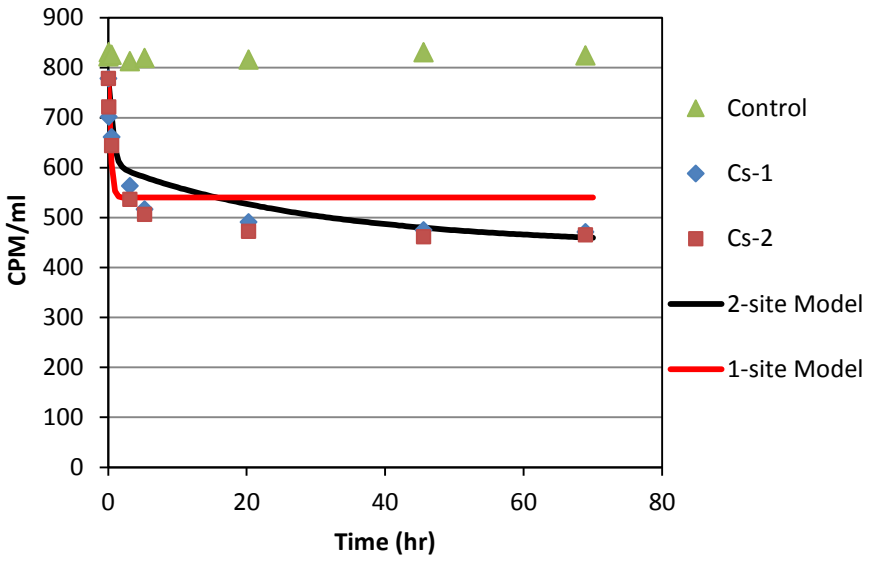

Figure 7-6. Results of batch adsorption experiment of ^{137}Cs onto FFM in SGW. 800 CPM/ml (starting concentration) corresponds to about 3e-11 M ^{137}Cs and about 9e-7 M total Cs. The one-site and two-site model curves were generated using the best-fitting parameters for the column experiments and do not represent fits to the batch data.

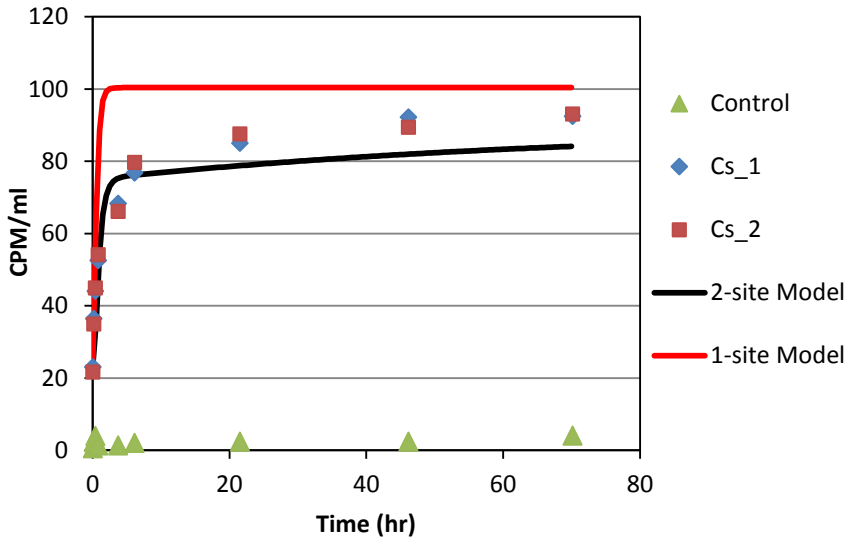

Figure 7-7. Results of batch experiment of first desorption step of ^{137}Cs from FFM in SGW. The one-site and two-site model curves were generated using the best-fitting parameters for the column experiments and do not represent fits to the batch data.

colloids were present. Furthermore, if one assumes that 25% of the solution-phase Cs in the colloid experiment is associated with the colloids (consistent with Cs partitioning to colloids in the absence of FFM), the concentration of dissolved Cs is nearly the same at the end of both experiments. The Cs-FFM K_d value at the end of this experiment is calculated to be approximately 320 ml/g, or nearly 6.5 times greater than the K_d value at the end of the adsorption experiment, and about 60% greater than at the end of the first desorption experiment. This result indicates that as successively more Cs is desorbed from the FFM, the remaining adsorbed Cs is, on average, more and more strongly associated with the FFM. Note

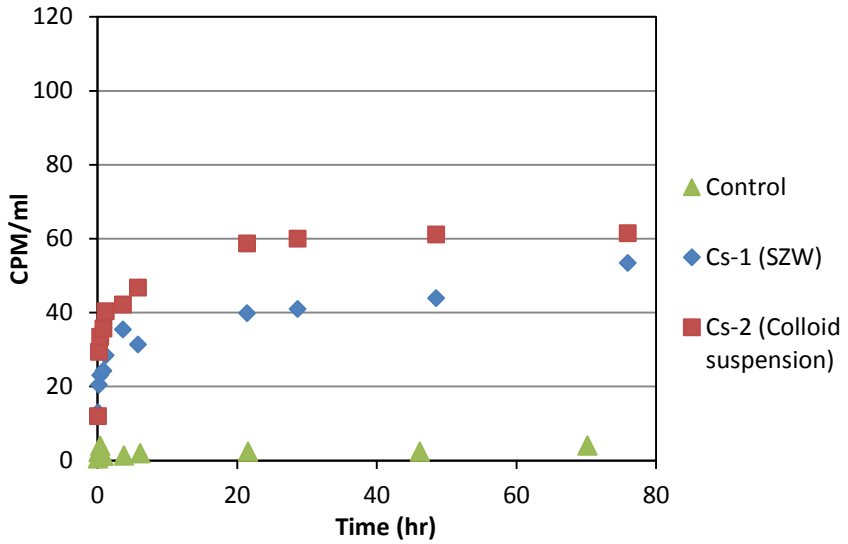

Figure 7-8. Results of batch experiment of second desorption step of ^{137}Cs from FFM in SGW (starting with FFM remaining after first desorption step shown in Figure 7-7). Note that the Cs-1 experiment involved desorption in colloid-free SZW, while Cs-2 involved desorption in SZW containing 100 mg/L of bentonite colloids. Model curves are not shown because there was no column experiment that corresponded to s second desorption step. The y-axis scale is the same as in Figure 7-7 to allow comparison of the amounts of ^{137}Cs desorbed.

that model curves are not shown in Figure 7-8 because the column experiments did not include the equivalent of a second desorption step.

Collectively, the batch experiment results suggest that there are multiple sorption sites on the FFM with different sorption and desorption rate constants and likely different sorption capacities. The batch data do not support a highly-refined determination of the rate constants and capacities of the different types of sites, but they certainly support the use of multiple sites when matching the column experiment data, which is important because it was found that the column data were much better matched when multiple sites were assumed.

7.4.2 Column Experiment Results

Figure 7-9 shows the Cs breakthrough curves in the FFM column experiments with and without colloids in the injection pulse. It is immediately apparent that the colloids transported through the column without significant filtration, as the colloid concentration jumped to its injection concentration (C/Co = 1) after one pore volume and remained there until the injection pulse ended. This result greatly simplified the modeling of the experiments, making it possible to assume a colloid filtration rate constant of zero. The mean water residence time in the columns, as determined from the ^{3}HHO breakthrough curves was approximately 1.5 hours, and the column Peclet number (column length divided by longitudinal dispersivity) was estimated to be around 100. Neither of these parameters were tightly constrained by the data because of the extremely rapid breakthrough of the ^{3}HHO, which resulted in only one to three samples being collected that contained C/Co values between 0 and 1.0.

The model fits to the Cs breakthrough curves in Figure 7-9 assume only a single type of sorption site on both the FFM and the colloids. However, the FFM sorption site was allowed to have a different desorption rate constant once the Cs and colloid injection pulse ended so that the hysteretic sorption behavior could be simulated. Changing the desorption rate constant effectively changed the K_d value because the K_d value is the ratio of the adsorption to the desorption rate constants. This adjustment is

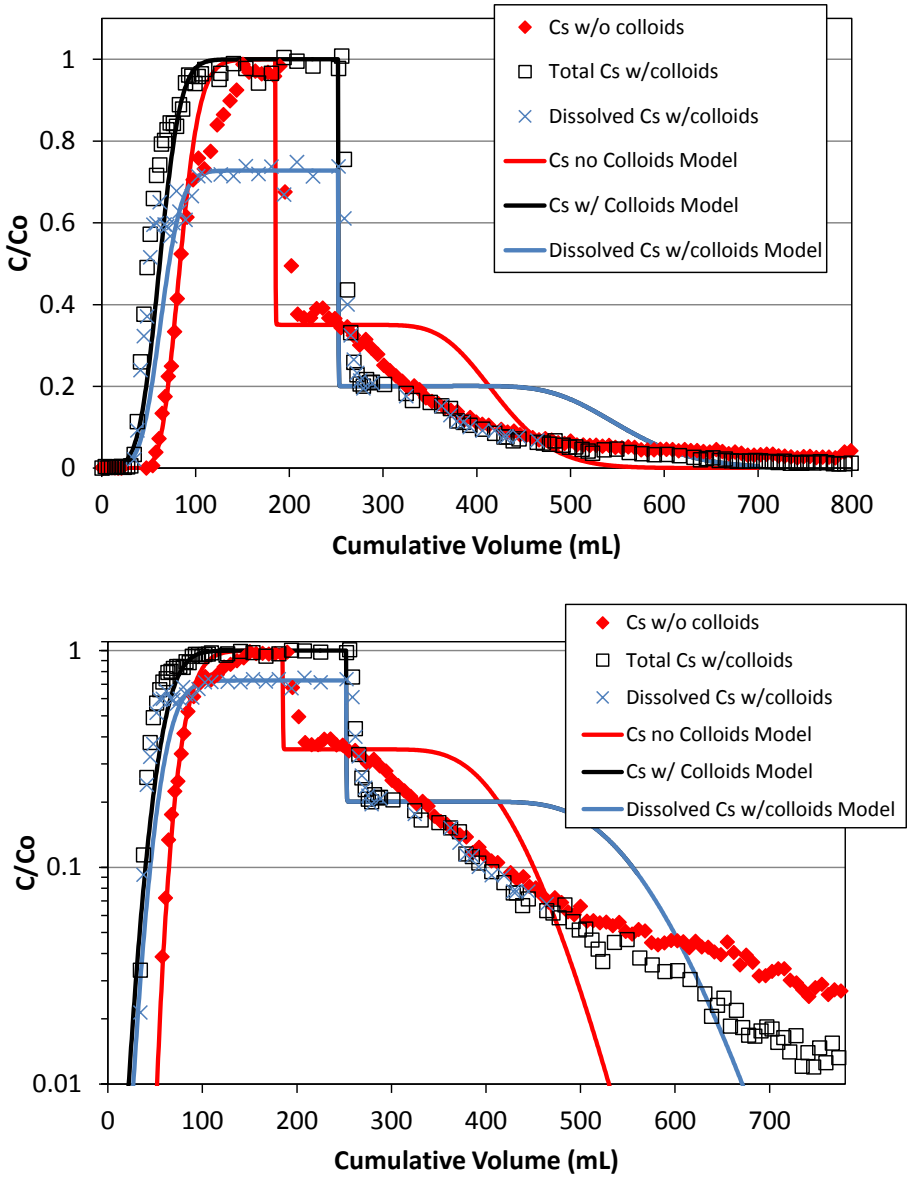

Figure 7-9. Normalized breakthough curves of ^{137}Cs in column experiments with and without colloids in the injection pulse (top – linear concentration scale; bottom - log concentration scale). Lines are model matches to the data assuming only a single type of sorption site on both the colloids and the FFM. Note that the injection pulses ended when the model curves show sudden drops in concentration. ^{3}HHO and colloid breakthrough curves are not shown, but the colloids essentially mirrored the ^{3}HHO curves and showed no evidence of any filtration. Model parameters are listed in Tables 7-5 and 7-6.

consistent with the hysteretic behavior observed in the batch sorption and desorption tests; in fact, it was initially assumed that the K_d values during adsorption and desorption in the column experiments were equal to the values deduced from the corresponding batch tests (with the desorption K_d value taken to be the K_d value observed at the end of the first batch desorption experiment, not the second one). These values were adjusted only slightly to achieve better matches to the column data.

It is apparent in Figure 7-9 that while the initial arrival and rising portion of the Cs breakthrough curves were matched reasonably well with a single sorption site, the desorption portions of the curves were poorly matched. The observed sudden drop in concentration at the end of the injection pulse can be matched quite well by adjusting the desorption rate constant. However, the larger desorption K_d value also results in a relatively steady concentration plateau for a much longer time than observed in the data, and then there is a much more rapid decline in concentration than the observed late-time tailing behavior. It should be noted that the K_d value for Cs partitioning to the bentonite colloids was fixed in all column simulations to be exactly that observed in the prepared colloid suspensions, i.e., 3700 ml/g. The rate constants for Cs partitioning to the colloids were allowed to vary to achieve better fits to the column data, but the ratio of the rate constants was fixed to be equal to the observed K_d value. The main constraint was that the rates had to exceed a lower threshold to avoid unrealistically early breakthrough of colloid-associated Cs.

As the model curves of Figure 7-9 suggest, it was not possible to obtain a reasonable match to the Cs tailing behavior in the column experiments using a single sorption site. Decreasing the desorption K_d value resulted in increasing the height of the concentration plateau, shortening the plateau, and steepening the eventual decline in concentration relative to the curves shown in Figure 7-9. Increasing the desorption K_d value had the opposite effect: it lowered and lengthened the plateau, and although it decreased the steepness of the eventual concentration decline, the decline was still considerably faster than the observed data. Attempts to manipulate the adsorption and desorption rate constants while keeping their ratios the same (i.e., keeping K_d values fixed) only marginally improved the matches to the desorption portion of the breakthrough curves, but it degraded the matches to the rising portion of the curves. The adsorption and desorption rate constants yielding the model curves of Figure 7-9 were used to obtain the one-site model curves for the batch experiments shown in Figures 7-6 and 7-7. It is apparent that these values provided reasonably good approximate matches to the batch data, although the rate constants that were assumed in the column experiments to avoid early breakthrough of Cs were clearly too fast to match the batch data.

Figure 7-10 shows the results of matching a two-site model (on both the FFM and colloids) to the column experiment Cs breakthrough curves with and without colloids present in the injection pulse. It is obvious that the two-site model offers a significant improvement over the one-site model, especially during the desorption portion of the column experiments. The inclusion of a second site with slower adsorption and desorption kinetics than the first site allows the Cs tailing behavior to be much better matched than when only a single site is allowed. Some discrepancies between the model and data remain in the early part of the desorption portion of the breakthrough curves, but these could be reduced by including a third sorption site on the FFM. We did not attempt to include a third site because we felt that the two-site model effectively captured the main features of the breakthrough curves. The adsorption and desorption rate constants and the sorption site capacities on the FFM yielding the model curves of Figure 7-10 are listed in Table 7-5. The one-site model parameters corresponding to the curves of Figure 7-9 are also listed in Table 7-5. The parameters of Table 7-5 were used to obtain the batch experiment model curves of Figures 7-6 and 7-7. It is apparent in Figures 7-6 and 7-7 that the two-site model parameters yielding good matches to the column transport data provided much better matches to the batch data than the one-site model parameters.

The colloid sorption site parameters assumed in all the model runs to interpret the column experiments are listed in Table 7-6. In the case where only a single sorption site on the colloids was assumed (Figure 7-9), the parameters for the second site were set to zero, but the same parameters were used for the first site regardless of whether a second site was assumed to be present or not.

It is worthwhile to make a couple of comments about the two-site model parameters of Tables 7-5 and 7-6. First, while a second sorption site is assumed on the colloids, this site has negligible impact on the model results because the capacity of the site is extremely small relative to the Cs concentrations in the experiments. The parameters of the second site were chosen to be consistent with the results of Missana

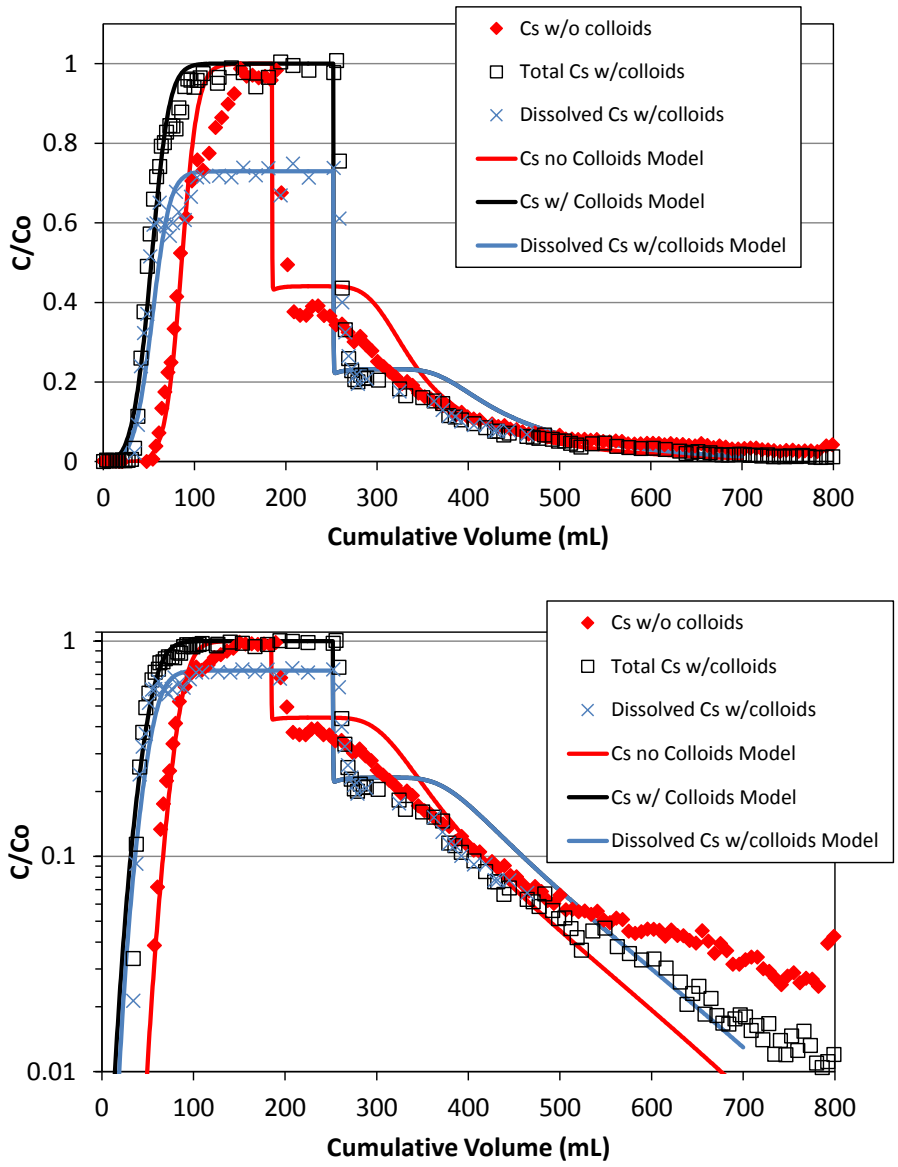

Figure 7-10. Normalized breakthough curves of Figure 7-9 showing model matches to the data assuming two types of sorption sites on both the colloids and the FFM. Model parameters are listed in Tables 7-5 and 7-6.

et al. (2004), who noted a strong Cs sorption site with very low capacity on FEBEX bentonite colloids in Grimsel groundwater, which was not apparent until Cs concentrations decreased below about 1e-8 M (Figure 7-1). The effective K_d values on the colloids as a function of Cs concentration using the two-site model parameters of Table 7-6 is shown in Figure 7-11; the similarity of this figure to Figure 7-1 is readily apparent.

Table 7-5. FFM sorption parameters yielding the model curves shown in Figures 7-9, 7-10, and 7-12.

Cs Transport with No Colloids						
	Figure 7-9 (1 site)		Figure 7-10 (2 sites)		Figure 7-12 (2 sites)	
Parameter	**Ads.**	**Des.**	**Ads.**	**Des.**	**Ads.**	**Des.**
Sorption rate constant, 1st site (ml/g-hr)	102	102	50	50	--	--
Desorption rate constant, 1st site (1/hr)	2	0.7	1.4	0.6	--	--
Max. site capacity, 1st site (mol/g)	1e-5	1e-5	1e-5	1e-5	--	--
Sorption rate constant, 2nd site (ml/g-hr)	--	--	1.02	1.02	--	--
Desorption rate constant, 2nd site (1/hr)	--	--	0.014	0.008	--	--
Max. site capacity, 2nd site (mol/g)	--	--	4e-8	4e-8	--	--
Cs Transport with Colloids						
	Figure 7-9 (1 site)		Figure 7-10 (2 sites)		Figure 7-12 (2 sites)	
Parameter	**Ads.**	**Des.**	**Ads.**	**Des.**	**Ads.**	**Des.**
Sorption rate constant, 1st site (ml/g-hr)	102	102	50	50	50	50
Desorption rate constant, 1st site (1/hr)	2	0.55	2	0.6	2	0.8
Max. site capacity, 1st site (mol/g)	1e-5	1e-5	1e-5	1e-5	1e-5	1e-5
Sorption rate constant, 2nd site (ml/g-hr)	--	--	1.02	1.02	1.02	1.02
Desorption rate constant, 2nd site (1/hr)	--	--	0.02	0.008	0.02	0.011
Max. site capacity, 2nd site (mol/g)	--	--	4e-8	4e-8	4e-8	4e-8

Note: Grey-shaded cells highlight increases in desorption rate constants in the presence of colloids during the adsorption phase of Figure 7-10 experiments (when colloids were present during adsorption phase), and green-shaded cells highlight increases in desorption rate constants in the presence of colloids during the desorption phase of Figure 7-12 experiment (vs. Figure 7-10 experiment where colloids were not present during desorption). Rate constants for the 1-site model (Figure 7-9) were adjusted to achieve good matches to the data without consideration of the presence or absence of colloids.

Table 7-6. Colloid sorption parameters used in all model simulations.

Parameter	Value
Sorption rate constant, 1st site (ml/g-hr)	29600
Desorption rate constant, 1st site (1/hr)	8
Max. site capacity, 1st site (mol/g)	1e-3
Sorption rate constant, 2nd site (ml/g-hr)	59200
Desorption rate constant, 2nd site (1/hr)	0.4
Max. site capacity, 2nd site (mol/g)	6e-8
K_d value, 1st site	3700
K_d value, 2nd site	148000

A second comment about the two-site model parameters of Tables 7-5 and 7-6 is that slightly larger desorption rate constants from the FFM (Table 7-6) were assumed during the adsorption portion of the column experiment with colloids than during the adsorption portion of the experiment without colloids. This adjustment was not arbitrary; it was made to honor the larger apparent desorption rate of Cs from the FFM in the presence of colloids than in the absence of colloids in the second batch desorption experiment (Figure 7-8). The relative difference in the desorption rate constants was approximately the same as that necessary to explain the difference in the two desorption data sets of Figure 7-8.

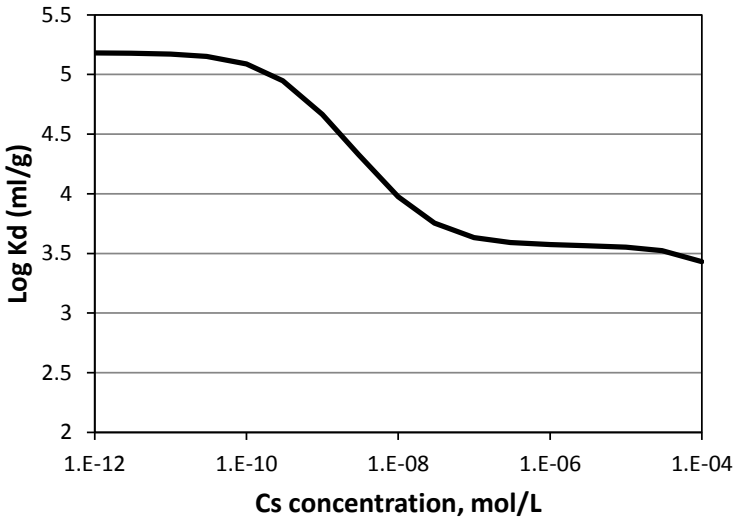

Figure 7-11. Cs K_d values on colloids as a function of Cs concentration using the sorption parameters of Table 7-6.

Figure 7-12 shows the breakthrough curves in the experiment in which a portion of the effluent from the column experiment containing colloids was injected into a second column. In this experiment, colloids continued to be injected after the end of the Cs injection pulse. This experiment was not modeled using a one-site model but rather was modeled using the same two-site model parameters as in the first column experiment involving colloids. The only difference in the model parameters between the two experiments was that a slightly larger Cs desorption rate constant from the FFM was assumed during the desorption portion of the second experiment to account for the increased desorption rate from the FFM in the presence of colloids (there were no colloids present during the desorption portion of the first experiment). It is apparent that there is good agreement between the model and data without any adjustment of the model parameters obtained from the first colloid experiment (other than the desorption rate constant adjustment to account for the presence of colloids during tailing in the second experiment). However, it is also apparent that if the model had been extended to longer times, it would have been necessary to include a third sorption site on the FFM to effectively capture the late-time tailing behavior.

An intriguing result of the second experiment was that the ratio of dissolved Cs to total Cs exiting the column became increasingly smaller as the tailing portion of the experiment progressed. Figure 7-13 shows this ratio as a function of eluted volume during the experiment, and Figure 7-14 shows the fraction as a function of total Cs concentration exiting the column, irrespective of time or volume eluted. These results are consistent with a second and stronger sorption site on the colloids that is just beginning to exert its influence as Cs concentrations decrease late in the experiment. That is, it is consistent with the results of Missana et al. (2004) that show evidence for a strong sorption site with low site abundance on the bentonite colloids that is apparent only at low Cs concentrations. The model curves of Figure 7-12 actually reflect a minor decrease in the ratio of dissolved to total Cs late in the experiment because of the inclusion of a second stronger sorption site on the colloids, but this decrease is not nearly as large as that observed in the experimental data.

Figure 7-15 shows the Cs recoveries as a function of volume eluted in each of the three column experiments. Over 90% of the Cs was recovered during each of the experiments, with the mass balance being closed to within a few percent by the final 0.1 M HCl flush. This flush confirmed that there was a small amount of remaining Cs in the columns at the end of each experiment.

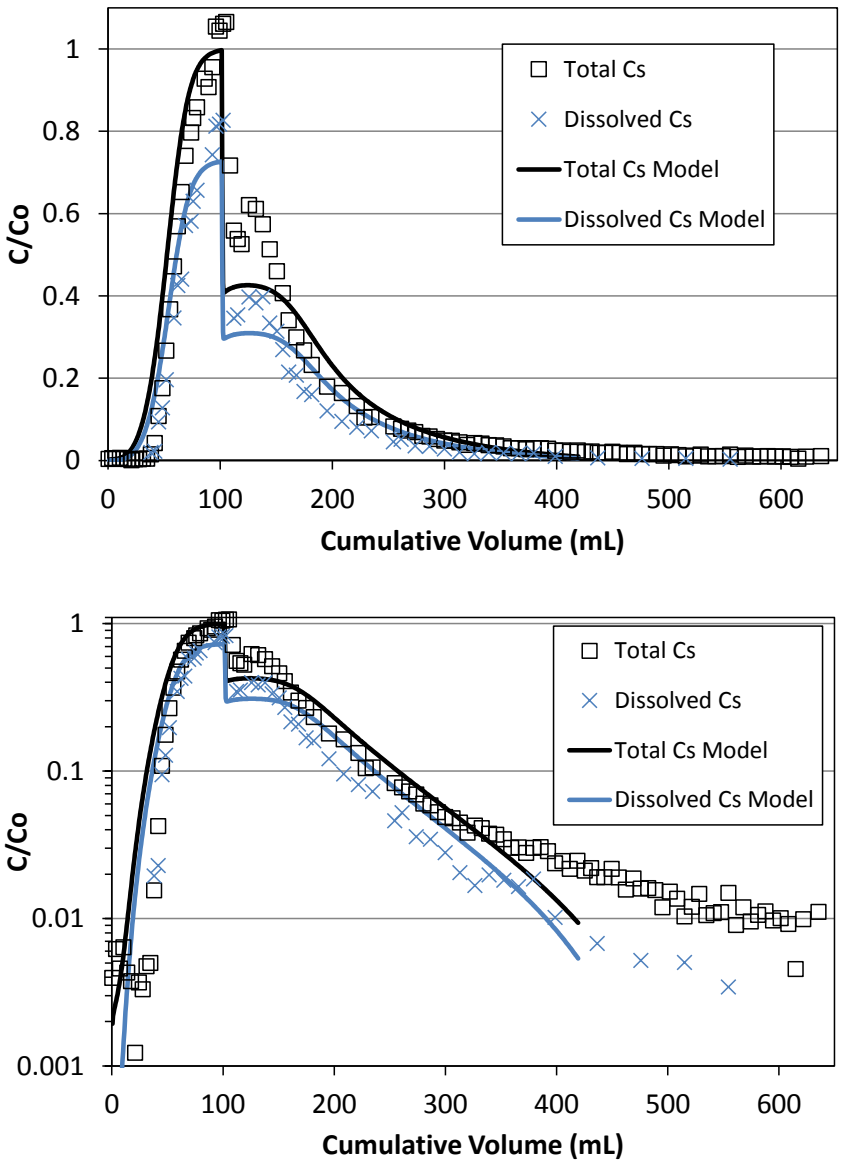

Figure 7-12. Normalized breakthough curves of ^{137}Cs in column experiment in which a portion of the effluent from the experiment with colloids shown in Figures 7-9 and 7-10 was passed through another column. Colloids continued to be injected through the column even after the Cs pulse had ended. Lines are model matches to the data assuming two types of sorption sites on both the colloids and the FFM. Note that the Cs injection pulse ended when the two model curves show sudden drops in concentration. ^{3}HHO and colloid breakthrough curves are not shown, but the colloids essentially mirrored the ^{3}HHO curves and showed no evidence of any filtration. Model parameters are listed in Tables 7-5 and 7-6.

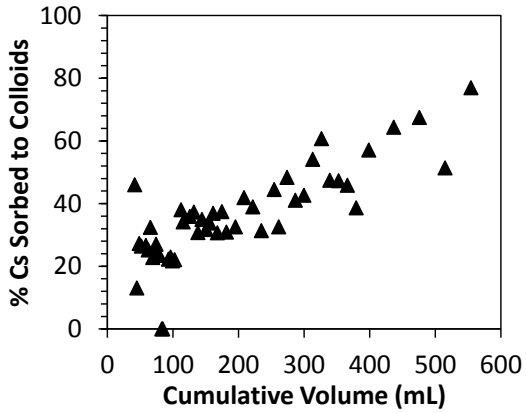

Figure 7-13. Fraction of Cs sorbed to colloids a function volume eluted in the experiments of Figure 7-12.

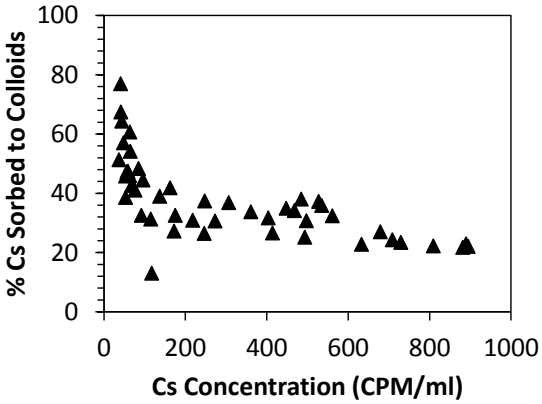

Figure 7-14. Fraction of Cs sorbed to colloids a function of Cs concentration in the experiments of Figure 7-12. Note that 50 CPM/ml is equivalent to about 5e-8 M total Cs concentration.

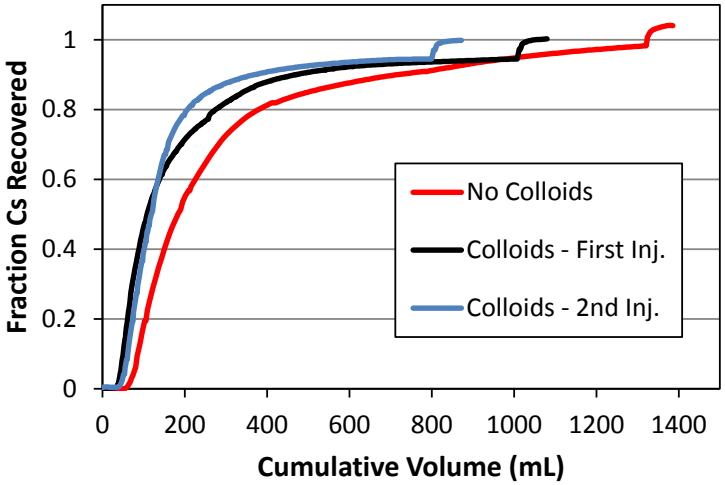

Figure 7-15. Fraction of Cs recovered in each of the column experiments.

7.4.3 Implications for Repository Performance Assessments

The implications of the batch and column experiments in this study are that Cs radioisotopes appear unlikely to transport over significant time and distance scales in association with bentonite colloids *unless* steady-state mobile colloid concentrations are quite high. Although Cs partitioning to the bentonite colloids is quite strong, the sorption process appears to be reversible, with the desorption kinetics being rapid enough that Cs would be expected to completely dissociate from mobile colloids over long time and distance scales that are relevant to repository performance assessments. We hasten to point out that greater facilitation of Cs transport by bentonite colloids would be expected if Cs concentrations were lower than in our experiments because of the stronger partitioning of Cs to the colloids at lower concentrations (observed by Missana et al., 2004, and also evident at late times in our second Cs/colloid column experiment). This greater Cs partitioning and slower desorption rates from bentonite colloids at lower Cs concentrations may have been responsible for the much greater apparent (relative to our experiments) colloid-facilitated transport of Cs in a 2012 GTS field transport experiment (described in Wang et al., 2013a), and in a 2002 GTS field experiment (Geckeis et al., 2004; Möri, 2004). In those field experiments, which were conducted in nominally the same geochemical system as our experiments, the colloid concentrations were comparable to ours (~100 mg/L), but the Cs concentrations were less than 1e-9 M, as opposed to about 1e-6 M in our experiments. The much lower Cs concentrations (due to the lack of non-radioactive carrier Cs associated with the ^{137}Cs) would have resulted in significantly stronger Cs partitioning to the colloids than in our experiments because of the much greater influence of the low-abundance strong sorption sites on the colloids at these lower Cs concentrations.

Under our experimental conditions of near-equilibrium Cs partitioning to both colloids and stationary media, as well as the nearly constant mobile colloid concentrations, the 1-D transport equation describing colloid-facilitated solute transport can be reduced to:

$$\frac{\partial C}{\partial t} + v_f \frac{\partial C}{\partial x} - D_c \frac{\partial^2 C}{\partial x^2} + \frac{\rho_f}{\eta} K_d \frac{\partial C}{\partial t} + K_c C_{col} \frac{\partial C}{\partial t} + v_f K_c C_{col} \frac{\partial C}{\partial x} = 0 \qquad (7\text{-}13)$$

which can be further simplified to:

$$\left(1 + \frac{\rho_f}{\eta} K_d + K_c C_{col}\right) \frac{\partial C}{\partial t} + \left(1 + K_c C_{col}\right) v_f \frac{\partial C}{\partial x} - D_c \frac{\partial^2 C}{\partial x^2} = 0 \qquad (7\text{-}14)$$

where K_c = equilibrium partition coefficient of the solute to the colloids, ml/g.

Equation (14) implies an effective solute velocity of $\left(1 + K_c C_{col}\right) v_f$ with a retardation factor of $1 + \frac{\rho_f}{\eta} K_d + K_c C_{col}$, so the overall effective retardation factor of the solute in the presence of the colloids, R_c, becomes:

$$R_C = \frac{1 + \frac{\rho_f}{\eta} K_d + K_c C_{col}}{1 + K_c C_{col}} \qquad (7\text{-}15)$$

Figure 7-16 shows the result of applying this simple expression in an analytical solution of 1-D advection-dispersion equation to predict the rising portion of the breakthrough curves of Figures 7-9 and 7-10. The measured values of K_d and K_c from the batch sorption experiments and the known colloid concentrations in the column experiments were used to calculate the colloid-facilitated transport retardation factor (eq. 7-15) and also the solute-only retardation factor, $R = 1 + \frac{\rho_f}{\eta} K_d$. It is apparent that these simple retardation

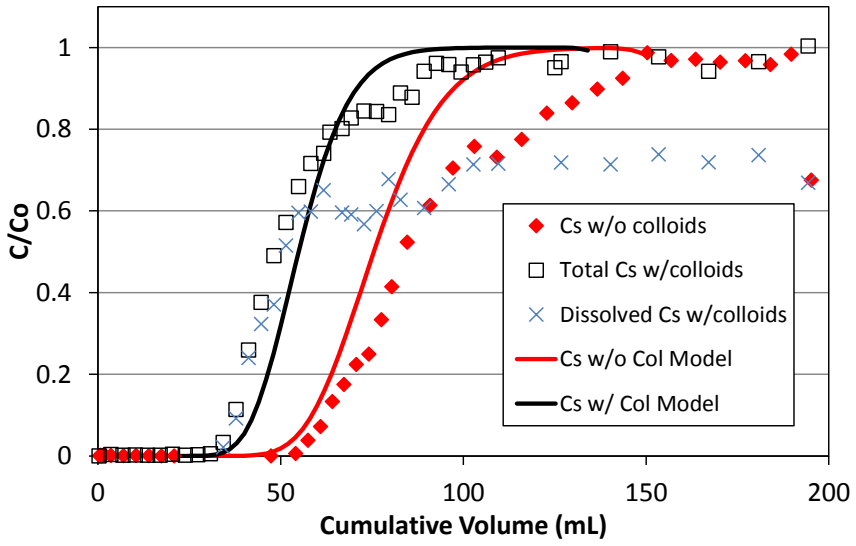

Figure 7-16. Predictions of the rising portion of the Cs breakthrough curves of Figures 7-9 and 7-10 using eq. (7-15) as a retardation factor for colloid-facilitated transport in an analytical solution of 1-D advection-dispersion equation. The K_d and K_c values from the batch experiments were used in eq. (7-15).

factors provide good predictions of the Cs breakthroughs in the column experiments. The analytical solution cannot be used to predict the desorption portion of the breakthrough curves because of the sorption-desorption hysteresis. Nevertheless, when solute partitioning to mobile colloids and immobile surfaces are fast and colloid concentrations are relatively constant, the retardation factor of eq. (15) can serve as a good approximation to estimate the potential for colloid-facilitated transport. Typically the value of $K_c C_{col}$ will be small compared to the value of $\frac{\rho_f}{\eta} K_d$ in the numerator of eq. (7-15) (in our experiments $K_c C_{col}$ was ~0.37 compared to about 200 for $\frac{\rho_f}{\eta} K_d$) because C_{col} is usually very small relative to $\frac{\rho_f}{\eta}$, so the main effect of the presence of colloids is in the denominator of eq. (7-15), where $K_c C_{col}$ must be greater than about 0.1 to have a significant impact on solute transport relative to transport in the absence of colloids.

7.5 Conclusions and Future Work

In this study, we demonstrate how a combination of batch sorption/desorption experiments and column transport experiments were used to effectively parameterize a model describing the colloid-facilitated transport of Cs in the Grimsel granodiorite/FFM system. Cs partition coefficient estimates onto both the colloids and the stationary media obtained from the batch experiments were used as initial estimates of partition coefficients in the column experiments, and then the column experiment results were used to obtain refined estimates of the number of different sorption sites and the adsorption and desorption rate constants of the sites. The desorption portion of the column breakthrough curves highlighted the importance of accounting for adsorption-desorption hysteresis (or a very nonlinear adsorption isotherm) of the Cs on the FFM in the model, and this portion of the breakthrough curves also dictated that there be at least two different types of sorption sites on the FFM. In the end, the two-site model parameters

estimated from the column experiments provided excellent matches to the batch adsorption/desorption data, which provided a measure of assurance in the validity of the model.

It was also demonstrated how a relatively simple retardation factor expression could be used to provide a good approximation of colloid-facilitated solute transport under conditions of near-constant mobile colloid concentrations and rapid and reversible solute sorption/desorption onto both the colloids and immobile surfaces. This expression provided a very good approximation to the column breakthrough curves using the partition coefficients observed in the batch experiments and the known colloid concentrations in the column experiments.

For future work, the model developed in this study will be applied to do a forward prediction of the Cs breakthrough curve in the 2012 colloid-facilitated transport experiment at the GTS. A previous interpretation of this experiment (Wang et al., 2013a) indicated that Cs transported much differently than in the laboratory experiments of this study. Desorption of Cs from the colloids in the field test was much slower than in the laboratory tests, resulting in an essentially unretarded breakthrough of a fraction of the injected Cs. There was no unretarded Cs transport in the lab column experiments despite the fact that the lab experiments had shorter residence times than in the field. The Cs partition coefficient to the colloids that provided a good match to the field Cs breakthrough curve was larger than for the stronger of the two sites in the laboratory-based model. However, it must be kept in mind that the Cs concentrations in the field experiment were lower than in the laboratory experiments by about three orders of magnitude, which would have increased the influence of the stronger sorption sites on the colloids. A goal of the future effort will be to refine the model and model parameters developed here to allow the model to explain both the laboratory and field Cs transport data. The key to this effort will be making adjustments to the parameters of the stronger of the two sorption sites on the colloids so that the strong site can account for essentially all of the Cs transport observed in the field test while the weaker site still accounts for most of the Cs transport observed in the laboratory tests. It may also be necessary to introduce an additional site to the model.

Additional future work for the Used Fuel Disposition Campaign (UFDC) in FY 2016 will include a comprehensive evaluation report on the state of knowledge of colloid-facilitated radionuclide transport as it applies to repository performance assessments. This effort will include interactions with performance assessment modelers on the project to develop an approach to efficiently account for colloid-facilitated transport in repository performance assessments. The evaluation report will include a summary of the results from this study as well as previous work in the UFDC program on the colloid-facilitated transport of americium in the Grimsel granodiorite system and the association of plutonium with intrinsic colloids (efforts at Lawrence Livermore National Laboratory), and it will also summarize and incorporate the results of field colloid-facilitated transport experiments at the GTS. The report will also draw heavily from numerous studies conducted outside the UFDC over the past 20+ years. A major emphasis of the report will be on how the collective observations and knowledge of colloid-facilitated radionuclide transport can be effectively upscaled to time and distance scales relevant to repository performance assessments.

7.6 References

Bertetti, F.P., Klar, R.V., and Vaught, M.M. (2006) *Colloid-Facilitated Transport of Radionuclides in Natural Groundwater Systems – Literature Rreview.* Report prepared for U.S. Nuclear Regulatory Commission by Center for Nuclear Waste Regulatory Analysis, San Antonio, TX.

Dittrich, T.M., Boukhalfa, H., Ware, S.D., and Reimus, P.W. (2015a). Laboratory investigation of the role of desorption kinetics on americium transport associated with bentonite colloids. *J. Environ. Radioactiv.* 148, 170-182. doi: 10.1016/j.jenvrad.2015.07.001

Dittrich, T.M., and Reimus, P.W. (2015). Uranium transport in a crushed granodiorite: Experiments and reactive transport modeling. *J. Contam. Hydrol*. 175-176, 44-59. doi: 10.1016/j.jconhyd.2015.02.004

Dittrich, T.M., Ware, S.D., and Reimus, P.W. (2015b). Mini-columns for conducting breakthrough experiments: Design and construction. *LA-UR-15-24392*; Los Alamos National Laboratory, Los Alamos, NM. doi: 10.2172/1184604

Dittrich, T. Gable, C.W., Hyman, J., Karra, S., Makedonska, N., Painter, S.L. and Reimus, P.W. (2014) Crystalline and Crystalline International Disposal Activities, Chapters 4 and 6, *FCRD-UFD-2014-000495*, prepared for Used Fuel Disposition Campaign of Fuel Cycle Research and Development, Los Alamos National Laboratory, Los Alamos, NM.

Dittrich, T.M., and P.W. Reimus. (2013). Experimental evaluation of actinide transport in a fractured granodiorite. *Proceedings of the 14th International High-Level Radioactive Waste Management Conference*, American Nuclear Society, LaGrange Park, IL. pp. 473-480.

Geckeis, H., Schäfer, T., Hauser, W., Rabung, Th., Missana, T., Degueldre, C., Möri, A., Eikenberg, J., Fierz, Th., and Alexander, W. (2004) Results of the colloid and radionuclide retention experiment (CRR) at the Grimsel Test Site (GTS), Switzerland – impact of reaction kinetics and speciation on radionuclide migration. *Radiochim. Acta*,. 92, 765-774.

Grolimund, D., Barmettler, K., and Borkevic, M. (2007) Colloid-facilitated transport in natural porous media: Fundamental phenomena and modelling, in *Colloid Transport in Porous Media*, Frimmel, F., von der Kammer, F, and Flemming, H-C., eds., Springer, Berlin, Germany.

Grolimund, D., and Borkevic, M. (2005) Colloid-facilitated transport of strongly sorbing contaminants in natural porous media: Mathematical modeling and laboratory column experiments, *Environ. Sci. Technol.*, 39, 6378-6386.

Huber, F., Kunze, P., Geckeis, H., and Schäfer, T. (2011) Sorption reversibility kinetics in the ternarysystem radiocuclide-bentonite colloids/nanoparticles-granite fracture filling material. *Appl. Geochem.*, 26, 2226-2237.

Iijima, K., Tomura, T., Tobita, M., and Suzuki, Y. (2010) Distribution of Cs and Am in the solution-bentonite colloids-granite ternary system: effect of addition order and sorption reversibility. *Radiochim. Acta* 98, 729-736.

Iijima, K., Shoji, Y., and Tomura, T. (2008) Sorption behavior of americium onto bentonite colloid. *Radiochim. Acta*, 96, 721-730.

Kanti, S.T. and Khilar, K.C. (2006) Review on subsurface colloids and colloid-associated contaminant transport in saturated porous media, *Adv. Colloid. Interface Sci.*, 119(2-3), 71-96.

Kersting, A. B. and P. W. Reimus, eds. 2003. "Colloid-Facilitated Transport of Low-Solubility Radionuclides: A Field, Experimental, and Modeling Investigation," *UCRL-ID-149688*, Lawrence Livermore National Laboratory, Livermore, CA.

Murali, M., and Mathur, J. (2002) Sorption characterisitics of Am(III), Sr(II) and Cs(I) on bentonite and granite. *J. Radioanal. Nucl. Ch*. 254(1), 129-136.

Painter, S., Cvetkovic, V., Pickett, D. and Turner, D.R. (2002) Significance of kinetics for sorption on inorganic colloids: Modeling and experiment interpretation issues, *Environ. Sci. Technol.*, 36, 5369-5375.

Wang, Y., et al. (2013a) Natural System Evaluation and Tool Development – International Collaborations: FY13 Progress Report, Used Fuel Disposition Campaign Milestone Report

FCRD-UFD-2013-000628; Chapter 2, Interpretations of Colloid-Facilitated Transport Experiments at the Grimsel Test Site from 2008 through 2012.

Wang, Y., Miller, A., Matteo, E., Reimus, P., Ding, M., Dittrich, T., Zheng, L., Houseworth, J., Zhao, P., Kersting, A., Dai, Z., and Zavarin, M., (2013b). *Experimental and Modeling Investigation of Radionuclide Interaction and Transport in Representative Geologic Media*, Chapter 5, An Experimental Methodology for Improving Radionuclide Transport Process Models Using Uranium and Grimsel Granodiorite as a Case Study. *FCRD-UFD-2013-000314*; pp. 47-76.